Temperature driven in-situ phase transformation of $PbWO_4$ nanobelts

Xue Wang,[1,2] Yong Ding,[1,a)] Zhong Lin Wang,[1] and Chenguo Hu[2]
[1]*School of Materials Science and Engineering, Georgia Institute of Technology, Atlanta, Georgia 30332-0245, USA*
[2]*Department of Applied Physics, Chongqing University, Chongqing, 400044, China*

(Received 28 March 2011; accepted 16 May 2011; published online 23 June 2011)

Monoclinic raspite $PbWO_4$ nanobelts were synthesized by a facile composite-salt-mediated method. By *in situ* heating to above 538 °C inside the chamber of a transmission electron microscope, the raspite nanobelts transformed irreversibly to tetragonal scheelite phase. By analyzing the experimental data, three possible topotactic transformation relationships between raspite and scheelite phases have been proposed. With further increasing the temperature up to 618 °C, part of the $PbWO_4$ nanobelts reduced to tetragonal WO_3 nanorods owing to the evaporation of Pb. © *2011 American Institute of Physics*. [doi:10.1063/1.3601500]

INTRODUCTION

The importance of lead tungstate ($PbWO_4$) crystals has been recognized recently due to its optical applications in high-energy physics, for example, in the development of new scintillators.[1–3] At room temperature, $PbWO_4$ has two different possible polymorphs, monoclinic raspite structure with space group $P2_1/c$, and tetragonal stolzite or scheelite structure with space group $I4_1/a$.[4] It is known that the raspite phase is a metastable and minority form under normal conditions.[5] With the increase of pressure, the tetragonal scheelite structure transforms into the monoclinic fergusonite structure at 9 GPa, and later to the monoclinic isostructural phase at 15 GPa.[6] Due to the difference in vapor pressure of the two oxides, WO_3 and PbO, $PbWO_4$ usually exhibits lead deficiency.[7] A super-lattice structure introduced by the Pb vacancy-ordering has been proposed,[8,9] but its existence remains unconfirmed.[7]

Scheelite $PbWO_4$ crystal can be grown using the traditional Czochralski melting technique,[10,11] while the appropriate methods to synthesize the raspite phased structures were just developed recently.[12–15] The raspite $PbWO_4$ nanobelts can be synthesized by using charged dextran as a structure directing coordination molecular template.[13] With the assistance of PVP surface-capping agent, the bamboo-leaf-like raspite $PbWO_4$ nanostructures can be fabricated.[14] Alternatively, composite-salt-mediated synthesis method was introduced to prepare ultra-long $PbWO_4$ raspite nanobelts.[15]

From the structure point of view, in spite of the very small volume difference of 0.53% between the raspite and scheelite forms, the difference in the cation coordination is remarkable. As displayed in Fig. 1, which gives the atomic structures of both raspite and scheelite, the W atoms in the scheelite structure are at the tetrahedral sites and isolated from one another, whereas in the raspite phase, they approach one another along the *b* axis and two W atoms share two O ions to form a chain of edge-shared octahedra. Each Pb ion is surrounded by seven O ions in the raspite structure, whereas in the scheelite structure, the number of the surrounding O ions to each Pb ion is eight.[16] It was reported that the phase transformation from raspite to scheelite at around 400 °C is irreversible.[17] The displacement of O ions in such a phase transformation is considered small, while that of the cations is relatively large. Although the structural relationship between raspite and scheelite was suggested to follow $a_r = -b_s + c_s$, $b_r = a_s$, $c_r = b_s$ (*r* raspite, *s* scheelite),[4] there may not be experimental evidence to support such an assumption.

Here in this work, by heating the raspite $PbWO_4$ nanobelts to high temperature, up to 618 °C, inside the chamber of a transmission electron microscope, we tracked how the raspite structure transforms to scheelite. The phase transformation was triggered when the temperature reached 538 °C. After the phase transition, the whole nanobelt was still a single crystal, although the evaporation of Pb ions was detected. The original raspite $PbWO_4$ nanobelts grew uniquely along the $[010]_r$ direction; after the nanobelts switched to scheelite phase, there were several different growth directions detected. Such an observation indicates more than one topotactic transformation relationship between the raspite and

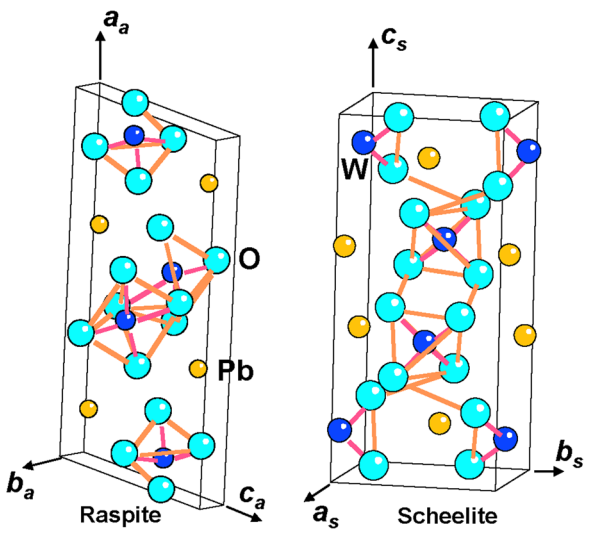

FIG. 1. (Color online) Atomic structures of $PbWO_4$ in raspite (left) and scheelite (right) forms.

a)Author to whom correspondence should be addressed. Electronic mail: yong.ding@mse.gatech.edu.

scheelite forms. With the temperature continuing to increase to 618 °C, with more Pb ions (and possibly O ions) lost, the nanobelts became polycrystalline. The x-ray energy dispersive spectra and electron diffraction both proved the formation of WO_3 nanorods from the $PbWO_4$ nanobelts. Two relationships between the scheelite $PbWO_4$ and WO_3 structures have been identified.

EXPERIMENTAL DETAILS

The raspite ultra-long nanobelts were synthesized by a composite-salt-mediated method without using any surface-capping agents. The detailed process can be found in Ref. 15. A Hitachi HF2000 transmission electron microscope equipped with a Gatan heating holder was used to carry out the *in situ* heating experiments. The scanning electron microscopy (SEM) images were recorded using a LEO 1530 SEM.

RESULTS

The lengths of the as-synthesized $PbWO_4$ nanobelts are up to hundred of microns and their widths are 200 nm to 2 μm. The SEM image in Fig. 2(a) shows their clear belt morphology. Figures 2(b) and 2(d) give two typical bright-field transmission electron microscopy (TEM) images of $PbWO_4$ nanobelts; their corresponding select-area electron diffraction (SAED) patterns are displayed in Figs. 2(c) and 2(e), respectively. The nanobelts are in raspite phase (Powder diffraction file (PDF) 00-016-0156) and they have unique growth or axial direction along $[010]_r$ and side surfaces as $(100)_r$ and $(001)_r$.

Figures 3(a) and 3(b) give the bright-field TEM images and the SAED pattern, respectively, of a $PbWO_4$ nanobelt at room temperature. The SAED pattern can be indexed with the electron beam along $[100]_r$ direction and the axial direction of the belt is along $[010]_r$. We heated the $PbWO_4$ nanobelt *in situ* inside the TEM high-vacuum chamber (3×10^{-6} Pa) to track the phase transformation. The temperature-increasing rate was around 50 °C per 10 min after the temperature reached 350 °C. The transformation was first identified when the temperature reached 538 °C. The image

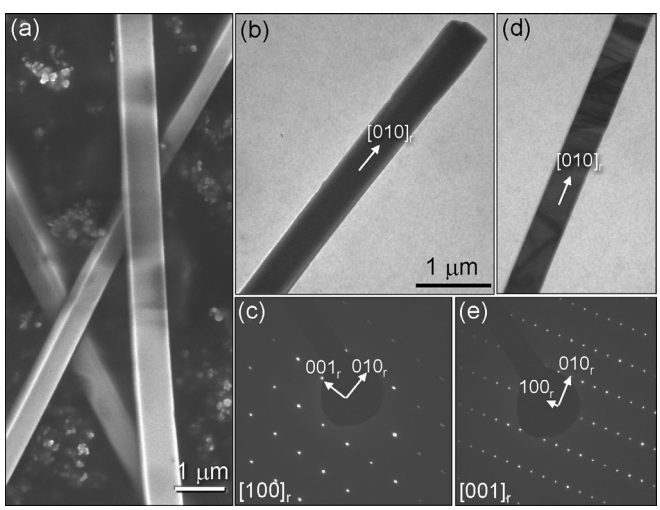

FIG. 2. (a) SEM image of raspite $PbWO_4$ nanobelts, (b) and (c) bright-field TEM images of raspite $PbWO_4$ nanobelts; their corresponding SAED patterns are shown in (d) and (e).

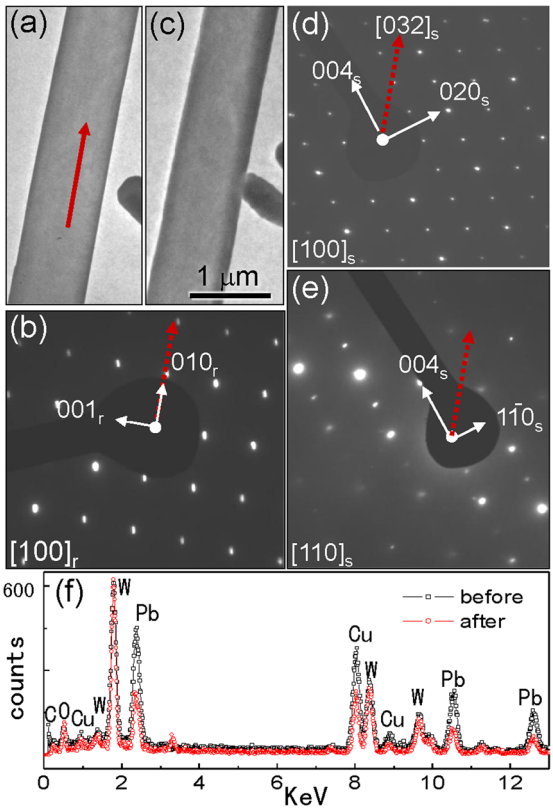

FIG. 3. (Color online) (a) and (c) TEM images from the same nanobelt recorded at room temperature and at 538 °C. (b) Its SAED pattern at room temperature. (d) and (e) SAED patterns from the nanobelt cooled down from 538 °C. (f) XEDS from the same belt before and after annealing at 538 °C.

contrast of the nanobelt did not change much as displayed in Fig. 3(c), which indicates that it was still a single crystal. However, dramatic changes occurred in its SAED patterns. Figures 3(d) and 3(e) are two SAED patterns recorded from the same nanobelt after the temperature cooled down from 538 °C; the titling angle between the two patterns is around 40°. Both diffraction patterns can be uniquely indexed by the scheelite structure (PDF 00-057-0836). The pattern in Fig. 3(d) is along the $[100]_s$ zone-axis while the one in Fig. 3(e) is close to the $[110]_s$ zone-axis. After the nanobelt switched to scheelite phase, the axial direction is close to the $[032]_s$ direction instead of the $\langle 100 \rangle_s$, as suggested by Fujita *et al.*[4] The x-ray energy dispersive spectra (XEDS) acquired from the nanobelt at room temperature and after annealing at 538 °C for 10 min are depicted in Fig. 3(f). Obviously, the scheelite nanobelt contains high-density Pb vacancies compared to their raspite counterpart. This can be understood from the different vapor pressures of the WO_3 and PbO at high temperature.

After increasing the temperature further to 618 °C, the surface roughness of the nanobelts can be observed, as shown in Fig. 4(a). Its SAED pattern is along the $[010]_s$ zone-axis, which is inserted in Fig. 4(a) as well. At this time, the axial direction of the nanobelt is close to $[100]_s$. Figure 4(c) is the SAED pattern from another nanobelt displayed in Fig. 4(b), which has a $[110]_s$ zone-axis. The axial direction of the belt has a ~15° angle to the $[001]_s$ axis.

In a short summary, we have checked more than ten nanobelts after heating to high temperature; the dominant

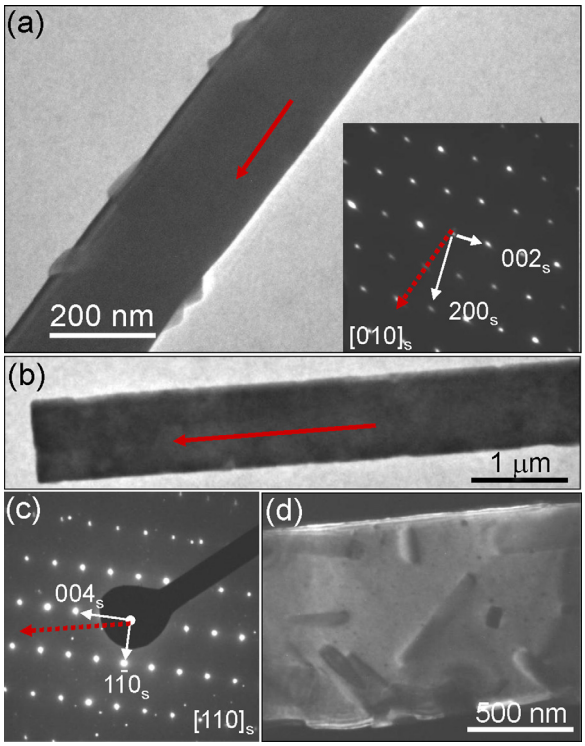

FIG. 4. (Color online) Two $PbWO_4$ nanobelts annealed at 618 °C and their corresponding SAED patterns. The arrowheads give the axial directions of the belts. (d) a dark-field TEM image of the nanobelt showing in (b).

axial direction of nanobelts is close to $\langle 100\rangle_s$ as assumed, some are close to $[001]_s$ axis, and one is close to $[032]_s$ as showing in Fig. 3. Considering the original axial direction in the raspite is along the $[010]_r$, there must have more than one possible approach to transform the raspite to scheelite structure. We will discuss this later.

If we examine the pattern in Fig. 4(c) carefully, there are some extra diffraction spots not belonging to the pattern of $[110]_s$ zone-axis, indicating that the nanobelt is not a single crystal anymore. These extra diffraction spots actually come from some rod shaped precipitates, which can be seen clearly in its dark-field image in Fig. 4(d).

The nanobelt in Fig. 5(a) contains these precipitated nanorods as well. Figure 5(b) is the dark-field TEM image recorded from the rectangle-enclosed area in Fig. 5(a). Most of the precipitated rods have a fixed ~45° angle with the axial direction of the nanobelt. The SAED pattern from the areas enclosed in circles C, D, E, and F in Fig. 5(a) are displayed, separately, in Figs. 5(c), 5(d), 5(e), and 5(f). The pattern in Fig. 5(c) belongs to the scheelite structure and can be indexed as $[001]_s$ zone-axis. The red arrowhead gives the axial direction, which is very close to $[100]_s$. The patterns in Figs. 5(e) and 5(f) are from the two precipitated rods and cannot be indexed by the $PbWO_4$ scheelite structure. While the pattern in Fig. 5(d) contains two sets of patterns, one is the same as the one shown in Fig. 5(c), the other is the same as the one displayed in Fig. 5(f). In order to indentify the phase of the rods, we acquired the XEDS from the rod enclosed in circle F and displayed it in the bottom part of Fig. 5(g). Compared to the XEDS acquired from the area enclosed in circle D (the top part in Fig. 5(g)), there are no detectable Pb signals in the rod. Considering only W and O in the rods, the SAED pattern in Figs. 5(e) and 5(f) can be indexed using the tetragonal WO_3 structure with space group P4/nmm (PDF 04-007-0954). [100] and $[1\bar{1}0]$, respectively, are the zone-axes of the SAED patterns in Figs. 5(e) and 5(f).

DISCUSSION

The raspite belongs to monoclinic structure with $a_r = 13.53$ Å, $b_r = 4.97$ Å, and $c_r = 5.55$ Å. Scheelite takes tetragonal structure with $a_s = b_s = 5.46$ Å and $c_s = 12.05$ Å. The projections of both raspite and scheelite structures in different orientations can be found in Fig. 6. Although the volumes of the unit cell of both raspite and scheelite forms are quite close, the cation coordination changes dramatically between them. In raspite, each W ion sits inside an O octahedron, and each octahedron share its edge with another two

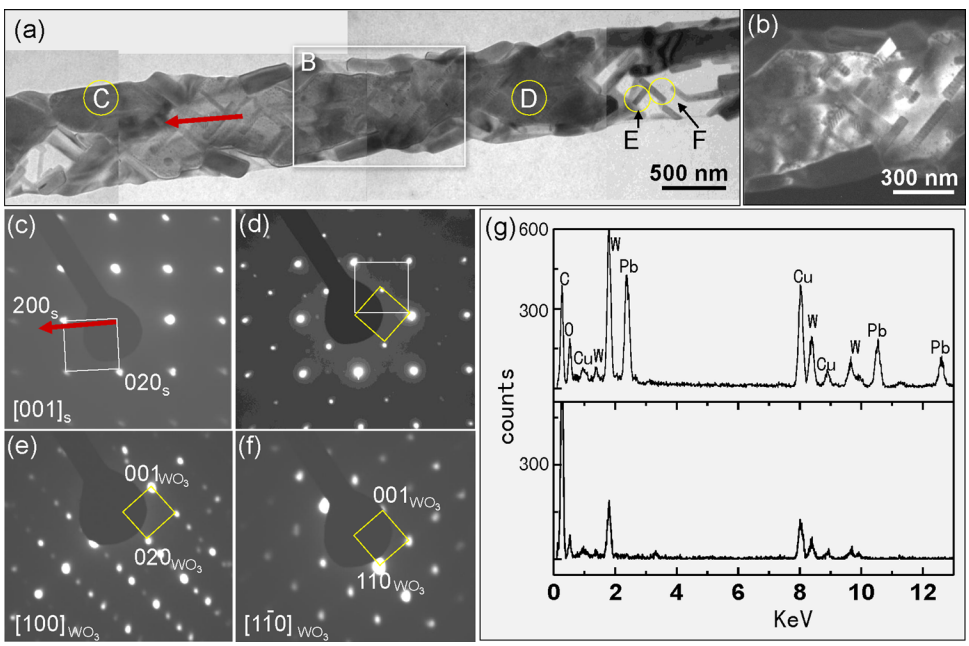

FIG. 5. (Color online) (a) A nanobelt showing precipitated WO_3 nanorods. (b) Dark-field TEM image recorded from the rectangle-enclosed area in (a). (c), (d), (e), and (f) SAED patterns recorded from the areas enclosed in circles C, D, E, and F in (a). (g) XEDS acquired from the areas enclosed in circles D (top) and F (bottom).

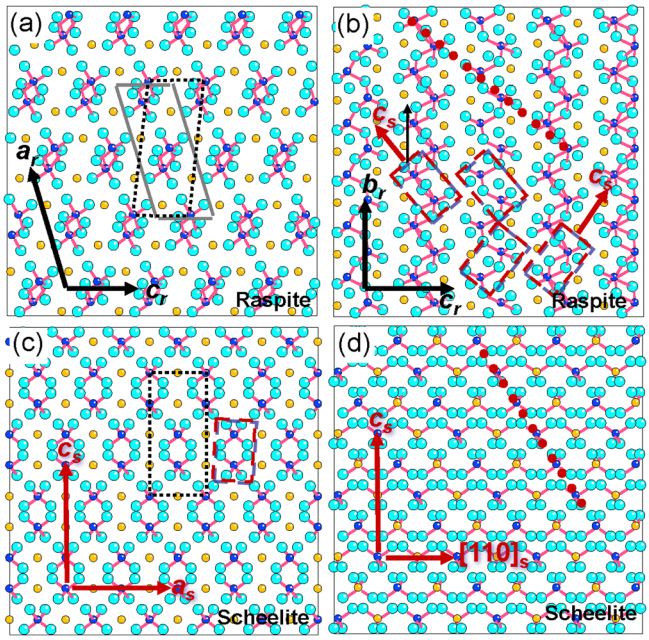

FIG. 6. (Color online) Projections of raspite PbWO4 structure in b_r axis (a) and a_r axis (b). Projections of scheelite $PbWO_4$ structure in b_s axis (c) and $[1\bar{1}0]_s$ axis (d). Dark solid and dotted lines mark the unit cells of raspite and scheelite forms. The dotted lines in (b) and (d) give the close-packed cation plane.

octahedra to form an octahedral chain along the $[010]_r$ directions. In scheelite, each W ion sits inside an O tetrahedron. These tetrahedra are not linked directly, but they approach one another along the c_s direction. Because the interatomic distance between Pb and O atoms is larger than that between W and O atoms, it is reasonable to regard that the Pb-O bonds are weaker compared to the W-O bonds, than the larger displacement of Pb ions after the phase transformation. Therefore, we will mainly focus on the W and O ions in the discussion of the $PbWO_4$ phase transformation.

One of the topotactic transformation relationships between raspite and scheelite was suggested by Fujita *et al.*,[4] as $a_r = -b_s + c_s$, $b_r = a_s$, $c_r = b_s$. This is indicated in Fig. 6(a), where the dark dotted lines show the distorted scheelite unit cell and the solid line gives the raspite one. This is actually the case, as we observed in Fig. 4(a) and Fig. 5(a). However, such a relationship cannot be used to understand the cases in Fig. 3 and Figs. 4(b) and 4(c). Based on the atomic structures, we proposed the second and third topotactic transformation relationships. The second one is represented as $(100)_s \parallel (100)_r$, $c_s \parallel [011]_r$, to explain the result we observed in Fig. 3; and the third one as $(1\bar{1}0)_s \parallel (001)_r$, $[\bar{1}\bar{1}1]_s \parallel [01\bar{1}]_r$ to explain the results in Figs. 4(b) and 4(c). In these two relationships, the displacement of W ions is considered small.

In the second relationship, as the red dashed lines highlighted in Fig. 6(c), we take the two nearby W-O tetrahedra along the c axis as the building block. Such a building block can be found in the raspite $[100]_r$ projection image in Fig. 6(b), where they are highlighted by red dashed lines as well.

The third relationship is based on the close packed cation planes. Such a plane is $\{111\}_s$ in the scheelite structure, while in raspite, it is close to $\{011\}_r$, as the dotted red line highlighted in both Figs. 6(b) and 6(d).

The two structural relationships between the $PbWO_4$ scheelite form and tetragonal WO_3 are illustrated in Fig. 7. The first is $(001)_s \parallel (100)_{WO3}$, $[110]_s \parallel [100]_{WO3}$, while the second is $(001)_s \parallel (1\bar{1}0)_{WO3}$, $[110]_s \parallel [110]_{WO3}$. The W ions sit in O tetrahedra in scheelite, while in WO_3, they move into O octahedra again as is the case in raspite, but differently; these octahedra are well separated in WO_3.

SUMMARY

By using *in situ* transmission electron microscopy, the heating driven phase transformation of $PbWO_4$ nanobelts has been investigated. The raspite to scheelite phase transformation was first identified at 538 °C and three topotactic transformation relationships have been proposed:

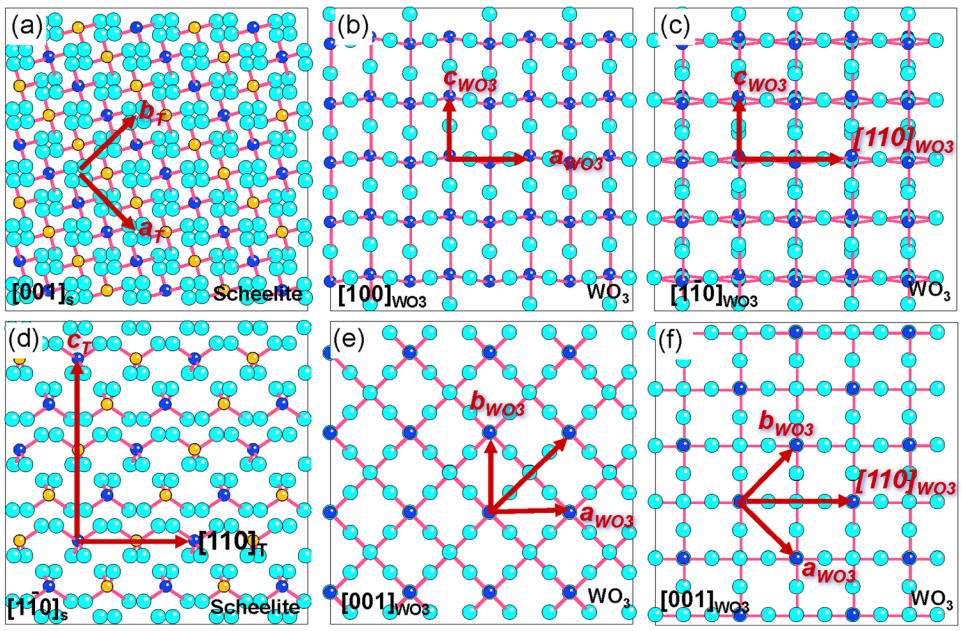

FIG. 7. (Color online) Projections of scheelite $PbWO_4$ structure and WO_3 structure along different axes. Corresponding to the [001] projected scheelite structure in (a), the two matching WO_3 structure are projected along [100] and $[1\bar{1}0]$, as shown in (b) and (c). The projections in (d), (e), and (f) are perpendicular to the ones in (a), (b), and (c), respectively.

(1) $a_r = -b_s + c_s, b_r = a_s, c_r = b_s$
(2) $(100)_s \parallel (100)_r, c_s \parallel [011]_r$
(3) $(1\bar{1}0)_s \parallel (001)_r, [\bar{1}\bar{1}1]_s \parallel [01\bar{1}]_r$.

With more Pb ions lost from the nanobelt with further increases in the temperature, WO_3 naorods will precipitate from the $PbWO_4$ nanobelts. Such WO_3 nanorods have two fixed structure relationships with their $PbWO_4$ matrix:

(1) $(001)_s \parallel (100)_{WO3}, [110]_s \parallel [100]_{WO3}$
(2) $(001)_s \parallel (1\bar{1}0)_{WO3}, [110]_s \parallel [110]_{WO3}$.

ACKNOWLEDGMENTS

X. W and CG. H thanks the funds support NSFC (60976055) and Postgraduates' Science and Innovation Fund (201005B1A0010339) of Chongqing University.

[1]P. Lecoq, Nucl. Instrum. Methods Phys. Res. A **537**, 15 (2005).
[2]A. N. Belsky, S. M. Klimov, V. V. Mikhailin, A. N. Vasilev, E. Auffray, P. Lecoq, C. Pedrini, M. V. Korzhik, A. N. Annenkov, P. Chevalier, P. Martin, and J. C. Krupa, Chem. Phys. Lett. **277**, 65 (1997).
[3]V. Kolobanov, N. Krutyak, M. Pashkovsky, and D. Spassky, Radiat. Meas. **42**, 887 (2007).
[4]T. Fujita, I. Kawada, and K. Kato, Acta Crystallogr. Sect. B: Struct. Sci. **33**, 162 (1977).
[5]R. Shaw and G. F. Claringbull, Am. Mineral. **40**, 933 (1955).
[6]D. Errandonea, J. Pellicer-Porres, F. J. Manjon, A. Segura, C. Ferrer-Roca, R. S. Kumar, O. Tschauner, J. Lopez-Solano, P. Rodriguez-Hernandez, S. Radescu, A. Mujica, A. Munoz, and G. Aquilanti, Phys. Rev. B **73**, 224103 (2006).
[7]R. Chipaux, G. Andre, and A. Cousson, J. Alloys Compd. **325**, 91 (2001).
[8]J. M. Moreau, P. Galez, J. P. Peigneux, and M. V. Korzhik, J. Alloys Compd. **238**, 46 (1996).
[9]J. M. Moreau, R. E. Gladyshevskii, P. Galez, J. P. Peigneux, and M. V. Korzhik, J. Alloys Compd. **284**, 104 (1999).
[10]K. Nitsch, M. Nikl, S. Ganschow, P. Reiche, and R. Uecker, J. Cryst. Growth **165**, 163 (1996).
[11]R. Oeder, A. Scharmann, D. Schwabe, and B. Vitt, J. Cryst. Growth **43**, 537 (1978).
[12]Y. Fang, Y. Xiong, Y. L. Zhou, J. X. Chen, K. P. Song, Y. Fang, and X. L. Zhen, Solid State Sci. **11**, 1131 (2009).
[13]J. H. Yang, C. H. Lu, H. Su, J. M. Ma, H. M. Cheng, and L. M. Qi, Nanotechnology **19**, 035608 (2008).
[14]T. George, S. Joseph, A. T. Sunny, and S. Mathew, J. Nanopart. Res. **10**, 567 (2008).
[15]C. H. Zheng, C. G. Hu, X. Y. Chen, H. Liu, Y. F. Xiong, J. Xu, B. Y. Wan, and L. Y. Huang, Cryst. Eng. Comm. **12**, 3277 (2010).
[16]L. S. Cavalcante, J. C. Sczancoski, V. C. Albarici, J. M. E. Matos, J. A. Varela, and E. Longo, Mater. Sci. Eng., B **150**, 18 (2008).
[17]M. Itoh and M. Fujita, Phys. Rev. B **62**, 12825 (2000).